In-Silico and In-Vitro Functional Validation of Imidazole Derivatives as Potential Sirtuin Inhibitor

Uma Maheswara Rao Dindi , Suhadha Parveen Sadiq , Sammer Al-Ghamdi , Naif Alrudian , Bin Dayelb Salman , Abdulwahab A. Abuderman , Shahidc Mohammad , Thiyagarajan Ramesh * , Ravikumar Vilwanathan *

Posted Date: 18 August 2023

doi: 10.20944/preprints202308.1350.v1

Keywords: Imidazole; Imidazole derivative; Sirtuins; NSCLC; Epigenetics

Article

In-Silico and In-Vitro Functional Validation of Imidazole Derivatives as Potential Sirtuin Inhibitor

Dindi Uma Maheswara Rao [1], Suhadha Parveen Sadiq [1] Sameer Al-Ghamdi [2], Naif Abdurhman Alrudian [2], Salman Bin Dayel [3], Abdulwahab Ali Abuderman [4], Mohammad Shahid [4], Thiyagarajan Ramesh [4,*] and Ravikumar Vilwanathan [1,*]

[1] Department of Biochemistry, Cancer Biology Laboratory, School of Life Sciences, Bharathidasan University, Tiruchirappalli- 620 024, Tamil Nadu, India.
[2] Department of Family and Community Medicine, College of Medicine, Prince Sattam Bin Abdulaziz University, Al-Kharj-11942, Saudi Arabia.
[3] Dermatology Unit, Internal Medicine Department, College of Medicine, Prince Sattam Bin Abdulaziz University, Al-Kharj-11942, Kingdom of Saudi Arabia.
[4] Department of Basic Medical Sciences, College of Medicine, Prince Sattam Bin Abdulaziz University, Al-Kharj-11942, Kingdom of Saudi Arabia
* Correspondence: Author's Address, Dr. Ravikumar Vilwanathan, Department of Biochemistry, Cancer Biology Laboratory, School of Life Sciences, Bharathidasan University, Tiruchirappalli- 620 024, Tamil Nadu, India. Email: ravikumarbdu@gmail.com; drvr@bdu.ac.in; Phone: +91-0431-2407071 (570); Fax: +91-0431-2407045; ORCID ID: 0000-0002-5134-6277; Dr. Thiyagarajan Ramesh, Department of Basic Medical Sciences, College of Medicine, Prince Sattam Bin Abdulaziz University, Al-Kharj-11942, Kingdom of Saudi Arabia; Email: r.thiyagarajan@psau.edu.sa

Highlights

1. Ethyl [5-(4-Chlorophenyl)-2-methyl-1H-imidazol-4-yl}-acetate was found to have a higher docking score, glide score, and glide energy when compared to other compounds sirtuin family proteins.
2. Ethyl [5-(4-Chlorophenyl)-2-methyl-1H-imidazol-4-yl}-acetate has higher stability during the itnteraction with sirtuins.
3. Imidazole derivative effectively reduces the viability of cancer cell lines A549 and NIC-H460 at lower concentrations compared to imidazole.
4. Ethyl [5-(4-Chlorophenyl)-2-methyl-1H-imidazol-4-yl}-acetate greatly affected the gene expression and protein expression of sirtuins family members.

Abstract: Sirtuins are a family of Class III epigenetic modifying enzymes involved in regulating cellular processes through the removal of acetyl groups from proteins. They rely on NAD^+ as a coenzyme in contrast with classical HDACs (Class I, II, and IV) that depends on Zn^+ for their activation, linking their function to cellular energy levels. There are seven mammalian sirtuin isoforms (SIRT1-7), each located in different subcellular compartments. Sirtuins act as master regulators of cellular homeostasis, responding to changes in nutrient availability and energy status. They play vital roles in diverse physiological and pathological conditions, making them promising therapeutic targets for various diseases, including cancer, neurodegenerative disorders, and metabolic diseases. High levels of SIRT6 are involved in the cancer progression of many tumor types and our previous studies revealed that sirtuin 6 was highly expressed in NSCLC cells and its inhibition potentially favored apoptosis and cell cycle arrest. Sirt6 emerged as a promising target and inhibitors of natural and synthetic sources are highly warranted. Imidazole derivatives are often investigated as sirtuin regulators due to their ability to interact with the binding site and modulate their activity. Imidazole bestows many possible substitutions on its ring and neighboring atoms, to design and synthesize derivatives with specific target selectivity and improved pharmacokinetic properties, optimizing drug development. We recently developed imidazole-based derivatives that potentially inhibited classical HDAC enzymes. Therefore, we evaluated the Sirtuin inhibition activity of our in-house compound

 doi:10.20944/preprints202308.1350.v1

comprised of imidazole derivatives and the strongest inhibition was observed with Ethyl 2-[5-(4-chlorophenyl)-2-methyl-1-H-Imidazole-4-yl) acetate against Sirt6 by in-silico and protein expression studies. Our results suggested that Ethyl 2-[5-(4-chlorophenyl)-2-methyl-1-H-Imidazole-4-yl) acetate could be a potential novel sirt6 inhibitor.

Keywords: imidazole; imidazole derivative; Sirtuins; NSCLC; epigenetics

1. Introduction

Imidazole derivatives have shown promising potential in combating various types of cancers. It can be designed and synthesized to specifically target molecular pathways and proteins that are crucial for the growth and survival of cancer cells [1,2]. This targeted approach minimizes damage to healthy cells and tissues, leading to fewer side effects. Imidazole derivatives have demonstrated the ability to inhibit cell proliferation and potentially induce apoptosis in lung cancer cells [3]. They can inhibit angiogenesis and by cutting off the blood supply to the tumor, these compounds can deprive the cancer cells of essential nutrients, hindering their growth [4]. Imidazole derivatives can sensitize cancer cells to the effects of chemotherapy and radiation therapy [5]. They have demonstrated better antimicrobial, antiviral, anti-inflammatory, antifungal, antiparasitic, and anticancer properties compared to other synthetic compounds [6]. The significance of imidazole derivatives lies in their diverse biological activities, structural versatility, and potential therapeutic applications. Implying the imidazole derivatives to study the epigenetic enzymes to modulate their activity and restore normal gene expression patterns is an active area of research [7]. The imidazole and its derivatives can either work as a friend or foe for the epigenetic enzymes. Our previous research emphasizes that the heterocyclic imidazole derivatives intervene in classic HDAC enzyme activity and inhibit their operations in the lung cancer cell lines [8]. But the class III, HDAC is the most active form in orchestrating the progression and suppression of the various disease [9]. With respect to Sirtuins, Imidazole derivatives can function as activators or inhibitors. Imidazole derivatives as activators of sirtuins can typically bind to the protein and increase their enzymatic activity, leading to enhanced deacetylation or ADP-ribosylation of target proteins. On the other hand, as an inhibitor, it can block Sirtuin activity, leading to altered gene expression patterns and cellular functions. Sirtuins play a crucial role in metabolic pathways, including glucose and lipid metabolism [10]. Activation of Sirtuins by imidazole derivatives or other compounds may enhance metabolic efficiency and potentially offer therapeutic benefits in metabolic disorders [11]. Sirtuins have been implicated in neuroprotection and cognitive function. Imidazole derivatives that modulate sirtuins activity may have potential applications in neurodegenerative diseases, such as Alzheimer's and Parkinson's, by promoting neuronal survival and enhancing cellular stress responses [12]. Sirtuins can act as tumor suppressors by regulating cell cycle progression, DNA repair, and apoptosis [13]. Sirtuin activators, including certain imidazole derivatives, may have anticancer properties by promoting tumor cell death and inhibiting tumor growth. Added, based on the cancer tissue types, the activity of Sirtuins keeps differing [14]. Developing effective and selective sirtuins regulators is a complex task.

The development of Sirtuin inhibitors as potential therapeutic agents for combating cancer, including lung cancer, is an active area of research [15]. Inhibiting specific sirtuin isoforms may offer opportunities for novel cancer treatments [16]. There are seven mammalian sirtuin isoforms (SIRT1-7), each with unique functions and subcellular localizations [17]. To develop effective inhibitors, it is crucial to understand the roles of individual sirtuin isoforms in lung cancer biology and identify those most relevant to disease progression. As Sirtuins actively participate in lung cancer progression and regulation [18], designing imidazole derivatives that can interfere with the activity of Sirtuin became the need of the hour. Structure-based drug design and screening approaches can be used to identify small molecules with potential inhibitory activity against sirtuin isoforms. Imidazole derivatives and other chemical scaffolds can be modified and optimized to interact with the NAD+-binding site of the

 doi:10.20944/preprints202308.1350.v1

target sirtuin isoform. Achieving isoform specificity is critical in the development of sirtuin regulators to avoid unwanted effects on non-target sirtuin isoforms, which may have distinct roles in normal cellular functions. Multiple in-house derivatives of Imidazole were synthesized, but their action upon the Sirtuins was unclear. Thus, our present study intends to develop potential imidazole derivatives which can interact with sirtuin and regulate their activity to devour the development of tumors in the lungs.

2. Materials and Methods

2.1. Ligand Preparation

An imidazole and six imidazole derivatives were generated in the ligand library. ChemDraw was used to draw the 3D structures of the ligands. Optimization of the ligand structures using Maestro version 13.2.128, Release 2022-2 ligprep module was performed with the force field OPLS_2005.

2.2. Protein Preparation and Receptor Grid Generation

All six Sirtuin isoforms were considered in the in-silico study, except Sirt4. The PDB structures of Sirt1, Sirt2, Sirt3, Sirt5, Sirt6 and Sirt7 were recovered from RCSB as 4I5I, 4RMH, 4JSR, 6LJK, 3K35 and 5IQZ respectively. The proteins subjected to docking studies were pre-processed, optimized, removed water, and minimized using a protein preparation wizard. Annihilation of water molecules, non-essential atoms, and attached ligands was performed. Further preparation was performed by addition of missing atoms in the protein residues, fixing the alternate confirmations, and by adding hydrogen. Grid generation surrounding the binding site was achieved as per the protocol followed in Maestro version 13.2.128, Release 2022-2.

2.3. Glide Docking

Grid-based Ligand Docking with Energetics (GLIDE) Maestro version 13.2.128, Release 2022-2 was used to dock the desired imidazole derivatives with all the six protein PDB. The study is carried out to understand the interaction of protein and ligand molecules by ranking the ligand's interactive score and energy. SIRTs 1-7 proteins, except Sirt4 were docked against the imidazole derivatives. In correspondence to the docking score, glide score, and the glide energy of the ligand and the protein, poses were visualized using Maestro GUI.

2.4. Molecular Dynamic Simulation- Desmond

In accordance with the docking score, the top ligand bound to all the Sirtuins was subjected to MD simulation using Desmond program version 7.0 (academic version). An orthorhombic periodic box of dimension 10 Å3 with solvent TIP3P at force field OPLS_2005 was set and the neutralization of the system at stable pH was carried out by the addition of counter ions (Na+ and Cl−) to the system builder. The protein-ligand complex underwent minimization of energy and attained a pre-equilibrium state. Molecular dynamics simulations were conducted for a duration of 100 nanoseconds, utilizing a relaxation time of 1 picosecond and maintaining a consistent temperature of 300 Kelvin. Throughout the simulation, a series of 1000 frames were generated using a time step of 20 picoseconds, serving as the foundation for deriving average structures during the production phase. Additionally, the root mean square fluctuation (RMSF) and root mean square deviation (RMSD) were assessed for both the protein-ligand complex structure and the protein structure alone. This analysis aimed to investigate the dynamic stability of the complexes and was visualized by plotting RMSF and RMSD values against time.

 doi:10.20944/preprints202308.1350.v1

2.5. DFT Analysis

The electronic structural characteristics play a pivotal role in elucidating the molecular interactions governing small molecule dynamics, molecular structure, and quantum properties. To delve into this, the Gaussian 09 software package was employed to conduct Density Functional Theory (DFT) calculations on the primary ligand. Employing the B3LYP-D3 hybrid functional and the 6-311G**++ (2d, 2p) basis set, the calculation encompassed the determination of the Highest Occupied Molecular Orbital (HOMO) and Lowest Unoccupied Molecular Orbital (LUMO) energy levels, collectively known as frontier orbitals. The HOMO signifies the outermost electron of the ligand capable of donation upon binding to a protein, while the LUMO represents the region of the ligand with an affinity to accept electrons from the protein during complex formation. An essential metric, the energy gap (HOMO-LUMO), was computed to elucidate chemical potential, electron affinity, chemical stability, hardness, and the chemical potential of the ligand molecules.

2.6. ADME analysis

The imidazole structure was constructed using Chemdraw, and various interactable R groups were added to the side chains. The structures were then exported into .sdf files and read in Schrodinger Maestro software version 13.2.128(2022-2). The structures were analyzed using the Qikprop module to understand their chemical properties. All the compounds underwent ADME analysis where the molecular weight, number of hydrogen bonds accepted and donated, SASA, FOSA, FISA, Percentage of Human absorption, and the permeability to the gut, and brain were calculated. This details the ability of the domestic compounds for acquiring the qualities of being a promiscuous drug **(Table 2)**.

2.7. Cell culture maintenance:

The A549 (adenocarcinoma) and NCI-H460 (squamous cell carcinoma) human non-small-cell lung cancer cell lines used in this study were purchased from National Centre for Cell Science (NCCS) Pune, India. The reagents for cell culture such as Dulbecco's Modified Eagle's Medium (DMEM), Fetal bovine serum (FBS), 10X Phosphate Buffered Saline (pH 7.2), 10X Trypsin-EDTA, 100X penicillin streptomycin (pen/strep, pH 7.2) antibiotic solution from Hi-Media Laboratories, Mumbai, India. Cell culture plates were purchased from Wuxi NEST Biotechnology Co. Ltd, Jiangsu, China. The other plastic wares were purchased from Tarsons PVT LTD.

The complete medium which includes Dulbecco's Modified Eagle's Medium (DMEM), 10% fetal bovine serum (FBS), and 1% pen strep solution (combination of penicillin and streptomycin) was used for culturing the cells. The cultured cell lines were maintained in a CO_2 incubator at an atmospheric temperature of 37 °C and supplied with 5% CO_2.

2.8. Cell viability assay by MTT:

The half maximal inhibitory concentration (IC_{50}) is a quantitative measure of a substance (e.g., drug) to inhibit biological processes or biological components by 50%. MTT assay is a well-known assay to determine the IC_{50}. The cell lines grown in monolayer were trypsinized and pelleted. The cell pellet is dissolved in a complete medium. The cells were then counted using the Trypan blue and hemacytometer. Approximately 1×10^4 cells were seeded in 96-well plates and incubated for overnight in a CO_2 incubator. After incubation, the old media was removed and serum-free media is added to the wells. The cells were then treated with different concentrations of imidazole ranging from 100µM to 1000µM and its derivative Ethyl [5-(4-Chlorophenyl)-2-methyl-1H-imidazol-4-yl]-acetate concentration ranging from 50µM to 500µM and incubated for 24 h. After the 24 h of treatment, 20ul of 5 mg/mL concentration of MTT (3 (4,5-Dimethyl-2-thiazolyl)-2,5-diphenyl-2H-tetrazolium bromide) is added to the wells, and incubated for 4 h. Later, the media is removed from the wells and 200 µL of Dimethyl sulphoxide (DMSO) is added to dissolve the formazan crystals. After 30 mins of incubation, the intensity of the purple color formed is measured by an ELISA plate reader (Bio-Rad Laboratories, Hercules, CA, USA) at 595nm. The higher the intensity, the greater number of viable cells, and the lower

Preprints (www.preprints.org) | NOT PEER-REVIEWED | Posted: 18 August 2023 doi:10.20944/preprints202308.1350.v1

the intensity, the lesser number of viable cells. MTT (RM1131) and DMSO (GRM5856) are purchased from Hi-Media Laboratories, Mumbai, India. The percentage of viable cells is calculated by the following formula.

% Cell viability = 100 – [(Mean OD of control cells – Mean OD of treated cells)/ Mean OD of control cells X 100]

2.9. Quantitative Real-time PCR (qRT-PCR):

The NSCLC cell lines A549 and NIC-H460 cells were seeded into culture plates using the complete medium. When the culture reached 80% confluency, the cells were treated with imidazole derivative Ethyl [5-(4-Chlorophenyl)-2-methyl-1H-imidazol-4- yl]-acetate. The IC_{50} concentration of Ethyl [5-(4-Chlorophenyl)-2-methyl-1H-imidazol-4- yl]-acetate in serum-free medium is used for treatment. Whereas the control maintained in serum-free medium without Ethyl [5-(4-Chlorophenyl)-2-methyl-1H-imidazol-4- yl]-acetate is used as control. After the treatment period, Total RNA was isolated from untreated (control) and Ethyl [5-(4-Chlorophenyl)-2-methyl-1H-imidazol-4- yl]-acetate treated A549 and NIC-H460 cell lines using TRIzol reagent (RNA isoplus). The Purity and quantity of the total RNA isolated was determined by BioPhotometer (Eppendorf, Hamburg, Germany). 1 µg of total RNA is taken for cDNA construction using PrimeScript RT reagent kit with manufacturer's instructions. The gene expression studies are performed in StepOnePlus real-time PCR system (Applied Biosystems, Thermos fisher scientific, MA, USA) using 2× SYBR green master mix SYBR green (TB Green Premix Ex Taq II (Tli RNase H Plus). The sample preparation is done according to the instruction in the data sheet provided by the manufacturer. 0.5 µl of cDNA is used for each 10 µl reaction. The PCR condition is initial denaturation at 94 ◦C for 5 min, followed by 40 cycles with denaturation at 94 ◦C for the 30s, annealing at 55 ◦C to 60 ◦C for the 30s (depending on specific gene), and melt curve stage condition's; 95 ◦C for 15s, 60 ◦C for 60s, 95 ◦C for 15s. The relative mRNA expression is calculated using the comparative threshold cycle (Ct) method (2-ΔΔCt). Glyceraldehyde 3-phosphate dehydrogenase (GAPDH) was used as an endogenous control. The list of primers used in this study is provided in **Table 1** [19]. Trizol for total RNA extraction (RNA isoplus, Cat. # 9108), PrimeScript RT reagent kit (Perfect Real Time, Cat. # RR037A) for cDNA synthesis and SYBR green master mix (TB Green® Premix Ex Taq™ II (Tli RNaseH Plus, Cat. #RR820A)) for gene expression studies were purchased from Taka Bio Inc. (Japan).

Table 1. List of primers used in the studies.

S. No	Gene	Primer sequence 5′-3′	Annealing.Temp	Product Size
1	GAPDH	F′ P: ATGGGGAAGGTGAAGGTCG R′ P: GGGTCATTGATGGCAACAATATC	60	107
2	SIRT1	F′ P: ACCCAGCTCACCTTCTTT R′ P: CCCAGACTTTCCCACTCT	57	176
3	SIRT2	F′ P: CTCCCCTTCCAGCTTAAC R′ P: TGACACTCACCCCAAGAC	57	175
4	SIRT3	F′ P: GGGAGGGGTACAGTGAGG R′ P: GGGTGACAGAGCGAGATG	58.1	177
5	SIRT4	F′ P: TGGTCATTGCTGGTTTCC R′ P: AGGCAGAGGTTGTGGTGA	57	170
6	SIRT5	F′ P: GGCTTTGCTTTCCCTTAC R′ P: AACCTTGGCGATTAGACC	58.1	171
7	SIRT6	F′ P: TCCCATTGTCTAGCCTCA R′ P: GATGTCGGTGAATTACGC	58.1	181
8	SIRT7	F′ P: TCGGCTCCTCCCTTCTAC R′ P: GGGGGCACTTTAGGAACA	57	180

Preprints (www.preprints.org) | NOT PEER-REVIEWED | Posted: 18 August 2023 doi:10.20944/preprints202308.1350.v1

2.10. Western blot analysis:

The A549 and NIC-H460 cell lines grown in monolayer were treated with Ethyl [5-(4-Chlorophenyl)-2-methyl-1H-imidazol-4-yl]-acetate in serum-free medium and untreated cell lines in serum-free medium were used as control samples. After the treatment period, the cells are washed with ice-cold PBS twice. Later RIPA Lysis Buffer supplemented with protease and phosphatase inhibitor cocktails is added to the plates and incubated for 30mins in cold conditions. After the incubation time is over, the cell lysate is collected by scraping using the cell scraper and collected into 1.5ml tubes. The cell lysate collected was vortexed for 30min at different intervals maintaining cold conditions by keeping tubes in ice. Later the cell lysate was the was centrifugation at 12,000g for 20 min at 4 °C in the colling centrifuge and the supernatant containing the total protein was collected. The protein samples are quantified by Lowry's method. 50 µg of protein from whole protein samples are used for western blot analysis. The 50 µg whole protein was separated using SDS-PAGE (10% and 12% gels) and the separated proteins were transferred onto the nitrocellulose membrane by wet transfer. The membrane is blocked with 5% skimmed milk for 2 h. The membrane is then washed with 1× TBST for 5 min. The washing was done three times. After the TBST wash, the membrane is incubated overnight with specific primary antibodies at 4 ◦C. Once the overnight incubation is over the membrane was washed three times with 1× TBST for 5 min each for three times. The alkaline phosphatase-conjugated secondary antibody specific to the primary antibody was added and incubated for 4 h at 4 ◦C. After 4 h of incubation the membrane is washed with 1× TBST for 5 min each for three times. The blots were developed with BCIP/ NBT chromogenic substrate and images were scanned. ImageJ software (e (National Institutes of Health, Bethesda, MD, USA) is used to measure the intensity of the bands. The protein expression in fold change is calculated after normalizing with the endogenous control Beta Actin. RIPA Lysis Buffer System (sc-24948) for protein isolation is purchased from Santa Cruz (CA, USA). Nitrocellulose Membrane (0.45µm, cat.log1620115) and Precision Plus Protein™ Kaleidoscope™ Prestained Protein Standards (#1610375) are purchased from Bio-Rad Laboratories (Hercules, California, United States). The bovine serum albumin, skimmed milk powder, and all the other fine chemical used in the SDS and western blotting are purchased from Sisco Research Laboratories Pvt. Ltd. (SRL, Maharashtra, India). All the details regarding the antibodies used in the studies are listed in **Table 2**.

Table 2. List of Antibodies used in the studies:.

S. No	Antibody	Molecular weight (kDa)	Brand	Cat. Log
1	β-Actin	45	Novus Biologicals	MAB8929-SP
2	Rabbit Monoclonal primary SIRT 1	120	Cell Signaling Technology	9475
3	Rabbit Monoclonal primary SIRT 2	39,43	Cell Signaling Technology	12650
4	Rabbit Monoclonal primary SIRT 3	28	Cell Signaling Technology	5490
5	Rabbit Monoclonal primary SIRT 5	30	Santa Cruz Biotechnology	8782
6	Rabbit Monoclonal primary SIRT 6	36-42	Santa Cruz Biotechnology	12486
7	Rabbit Monoclonal primary SIRT 7	45	Santa Cruz Biotechnology	5360

 doi:10.20944/preprints202308.1350.v1

2.11. Statistical analysis

The graphical presentation of the data in this study is from biological replicates and presented as the mean ± SD done using ordinary one-way ANOVA with Tukey's multiple comparisons test by GraphPad Prism software (version 9.4.0, CA, USA). The Significance is represented as *p < .05 and **p < .01, ***p < .001 and ****p < .0001.

3. Results

3.1. Structure description

The structures of sirtuins retrieved from RCSB were scrutinized carefully. Multiple deposits of protein structure were found for all the Sirtuin isoforms. The PDB structures 4I5I(Sirt1), 4RMH (Sirt2), 4JSR(Sirt3), 6LJK(Sirt5), 3K35(Sirt6), and 5IQZ(Sirt7) were selected because of better resolution and with zero mutation and superimposed to analyze the similarity and efficiency against all the deposited structures using Pymol software. The binding pockets and the interactive amino acids present in the pockets were also visualized. While preparation of sirtuin protein, NAD^+ bound to the protein, and the essential Zn^+ metal was allowed to be present within the structure and the ligand of interest was docked against the binding site.

3.2. Molecular Docking

A molecular docking experiment was carried out using the glide software in which the selected Protein PDB is docked against the selected Imidazole derivatives. Glide incorporates various scoring functions to assess the binding affinities of ligands within the active site (**Figures 1 and 2**). These scoring functions consider factors such as van der Waals interactions, hydrogen bonding, electrostatic interactions, and hydrophobic interactions. Among all the compounds subjected to the docking, Ethyl 2-[5-(4-chlorophenyl)-2-methyl-1-H-Imidazole-4-yl) acetate shows higher docking score, glide score, and glide energy when compared to other compounds. Also, the compound has impressive interactions with all the sirtuins, with some concern for cellular localization **(Table 3)**.

Preprints (www.preprints.org) | NOT PEER-REVIEWED | Posted: 18 August 2023 doi:10.20944/preprints202308.1350.v1

Interaction between Ethyl 2-[5-(4-chlorophenyl)-2-methyl-1-H-Imidazole-4-yl) acetate with Nuclear Sirtuins

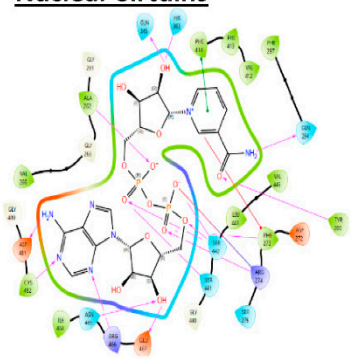

SIRT1

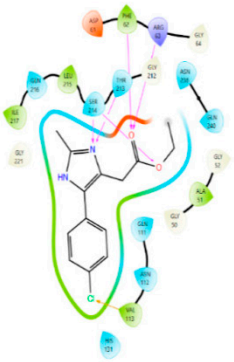

SIRT6

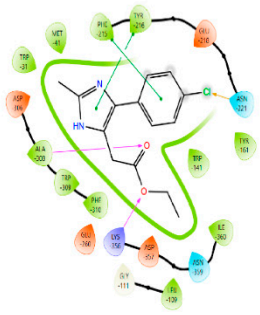

SIRT7

Interaction between Ethyl 2-[5-(4-chlorophenyl)-2-methyl-1-H-Imidazole-4-yl) acetate with Cytoplasmic Sirtuins

SIRT2

Interaction between Ethyl 2-[5-(4-chlorophenyl)-2-methyl-1-H-Imidazole-4-yl) acetate with Mitochondrial Sirtuins

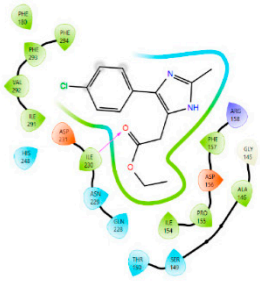

SIRT3

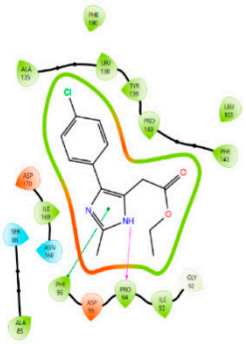

SIRT 5

Figure 1. Ligand interaction report after the docking analysis: The ligands bound to all the sirtuins-binding pocket is shown. The amino acids interacted and the hydrogen bond formed between the ligand-protein are also seen.

Preprints (www.preprints.org) | NOT PEER-REVIEWED | Posted: 18 August 2023 doi:10.20944/preprints202308.1350.v1

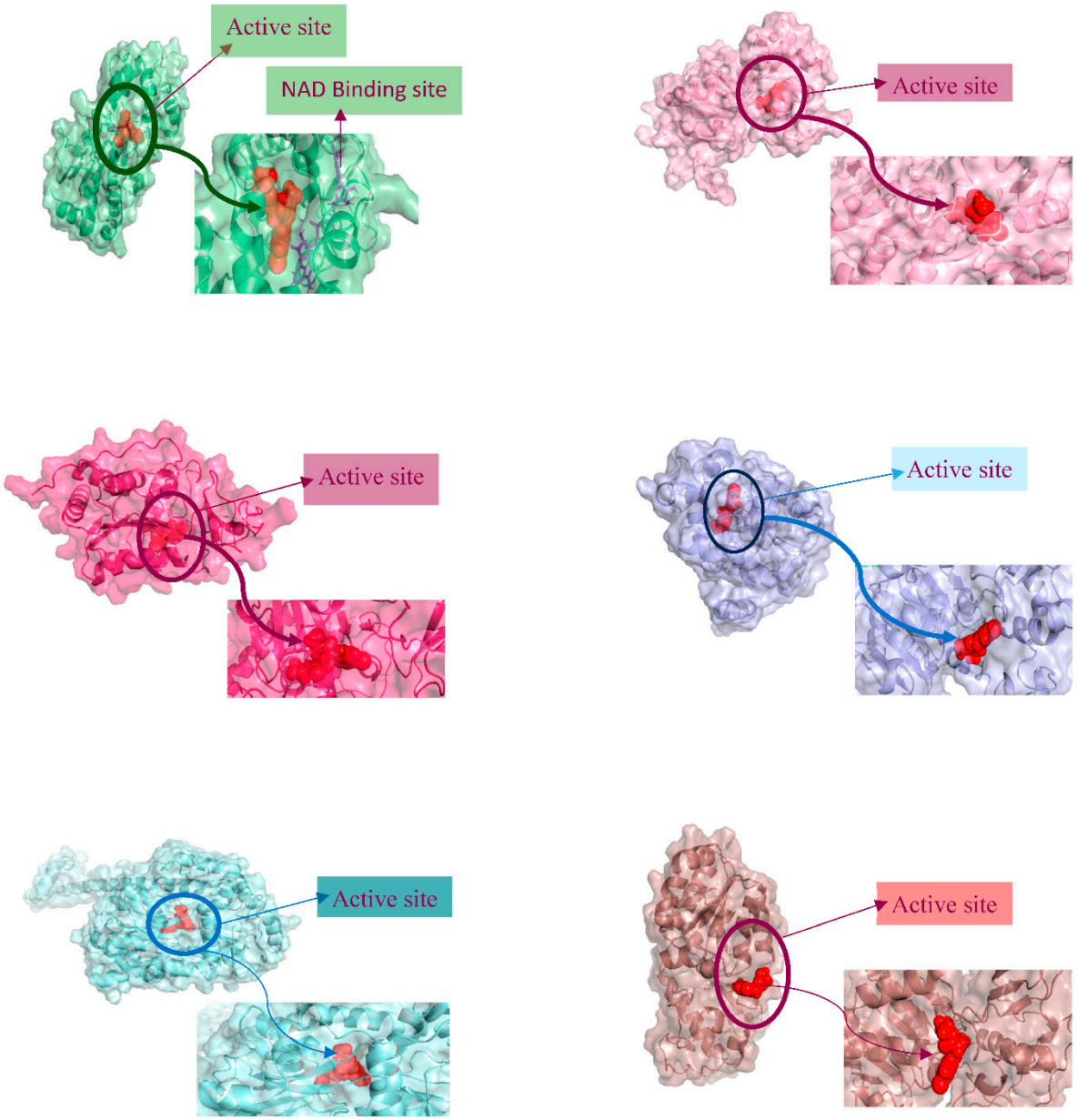

Figure 2. 3D View of Ligand Fit into the Binding Pocket of the Protein: The ligands bound to the active site of the protein is shown.

Table 3. Molecular docking analysis- Glide Module.

PDB	SIRT1 (4I5I)		SIRT2(4RMH)		SIRT3 (4JSR)		SIRT5(6LJK)		SIRT6(3K35)		SIRT7(5IQZ)	
Ligand Name	Glide Score	Glide Energy	Glide Score	Glide Energy	Glide Score	Glide Energy	Glide Score	Glide Energy	Glide Score	Glide Energy	Glide Score	Glide Energy
Ethyl 2-(2,5-diphenyl-1 imidazole-4-yl) acetate	-5.727	-18.208	-4.32	-14.778	-4.495	-17.511	-7.053	-15.008	-5.401	-19.483	-6.229	-41.320
Ethyl 2-[2-phenyl-5-(3,4,5-trimethoxyphenyl)-1H-imidazol-4-yl] acetate	-6.655	-28.841	-7.289	-39.668	-8.186	-54.470	-4.912	-35.961	-5.773	-47.432	-5.000	-41.870
Ethyl 2-[5-(4-chlorophenyl)-2-phenyl-1H-imidazol-4-yl] acetate	-7.556	-31.593	-9.056	-46.782	-7.019	-44.698	-5.735	-32.778	-5.225	-45.219	-5.498	-42.018
Ethyl 2-[5-(4-bromophenyl)-2-phenyl-1H-imidazol-4-yl] acetate	-7.742	-35.492	-8.816	-46.547	-7.442	-49.158	-4.686	-32.981	-4.664	-44.797	-5.404	-42.510
Ethyl 2-{2-phenyl-5-[4-(trifluoromethyl) phenyl]-1H-imidazol-4-yl} acetate	-9.656	-26.563	-7.711	-39.699	-7.714	-49.695	-5.584	-32.798	-4.825	-45.74	-5.558	-44.785
Ethyl 2-[5-(4-chlorophenyl)-2-methyl-1-H-Imidazole-4-yl) acetate	-7.807	-37.735	-8.835	-41.366	-7.053	-43.362	-5.053	-31.857	-6.544	-45.913	-5.616	-39.446
Imidazole	-5.723	-18.112	-4.318	-14.734	-4.495	-17.511	-5.277	-15.008	-5.385	-19.497	-4.092	-16.893

doi:10.20944/preprints202308.1350.v1

Preprints (www.preprints.org) | NOT PEER-REVIEWED | Posted: 18 August 2023 doi:10.20944/preprints202308.1350.v1

3.3. Molecular Dynamics

MDS run with 100ns simulation and 1000 frames generated a set of RMSD (Figure 3), RMSF (Figure 4), and protein-ligand interaction plots (**Figures 5 and 6**). Sirt1, sirt2, and sirt6 were found to have stable simulation ranges with the increase of nanoseconds. Other Sirtuins showed non-synchronous simulation stability.

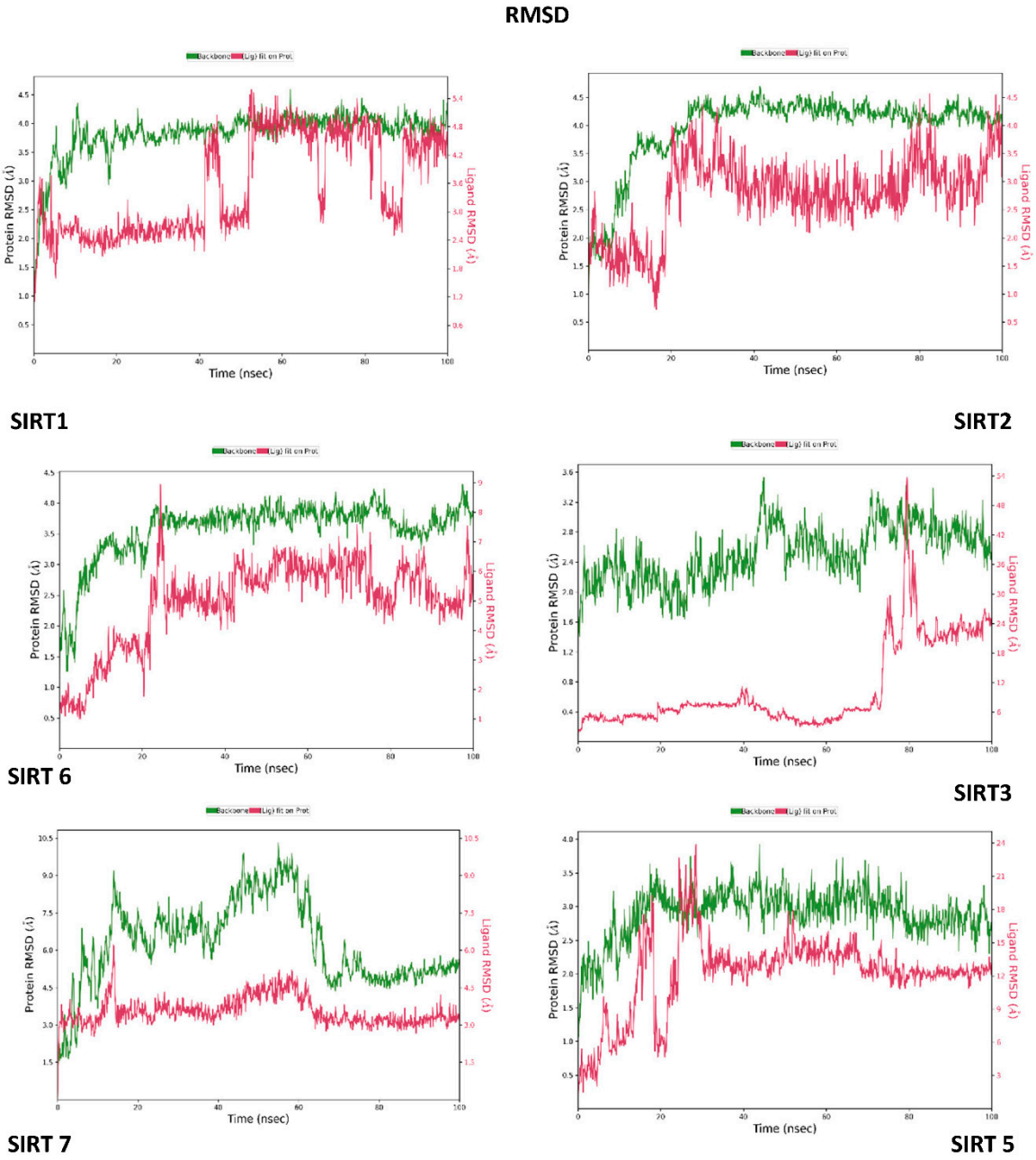

Figure 3. The Root Mean Square Deviation (RMSD) is a metric used to gauge the average change in atom displacement within a selected group of atoms in a specific frame, in comparison to a reference frame. This calculation is performed for all frames in a given trajectory. The presented plot illustrates the progression of RMSD for all the sirtuin protein (displayed on the left Y-axis in each graph plot). Meanwhile, Ligand RMSD (depicted on the right Y-axis) provides insight into the stability of the ligand concerning both the protein and its binding pocket.

Preprints (www.preprints.org) | NOT PEER-REVIEWED | Posted: 18 August 2023 doi:10.20944/preprints202308.1350.v1

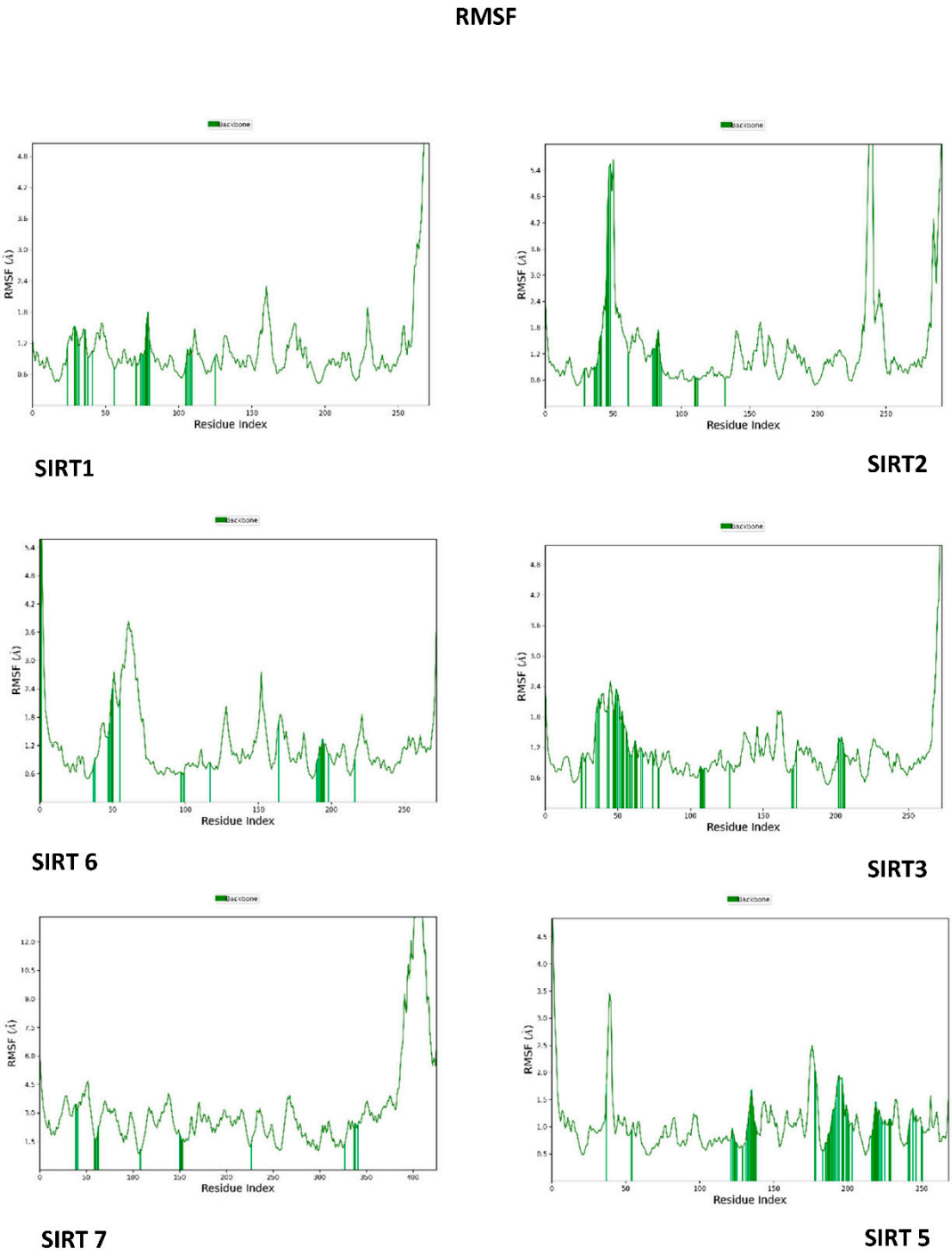

Figure 4. The Root Mean Square Fluctuation (RMSF) is useful for characterizing local changes along the protein chain. Sirtuin protein residues that interact with the ligand are marked with green-colored vertical bars.

Preprints (www.preprints.org) | NOT PEER-REVIEWED | Posted: 18 August 2023 doi:10.20944/preprints202308.1350.v1

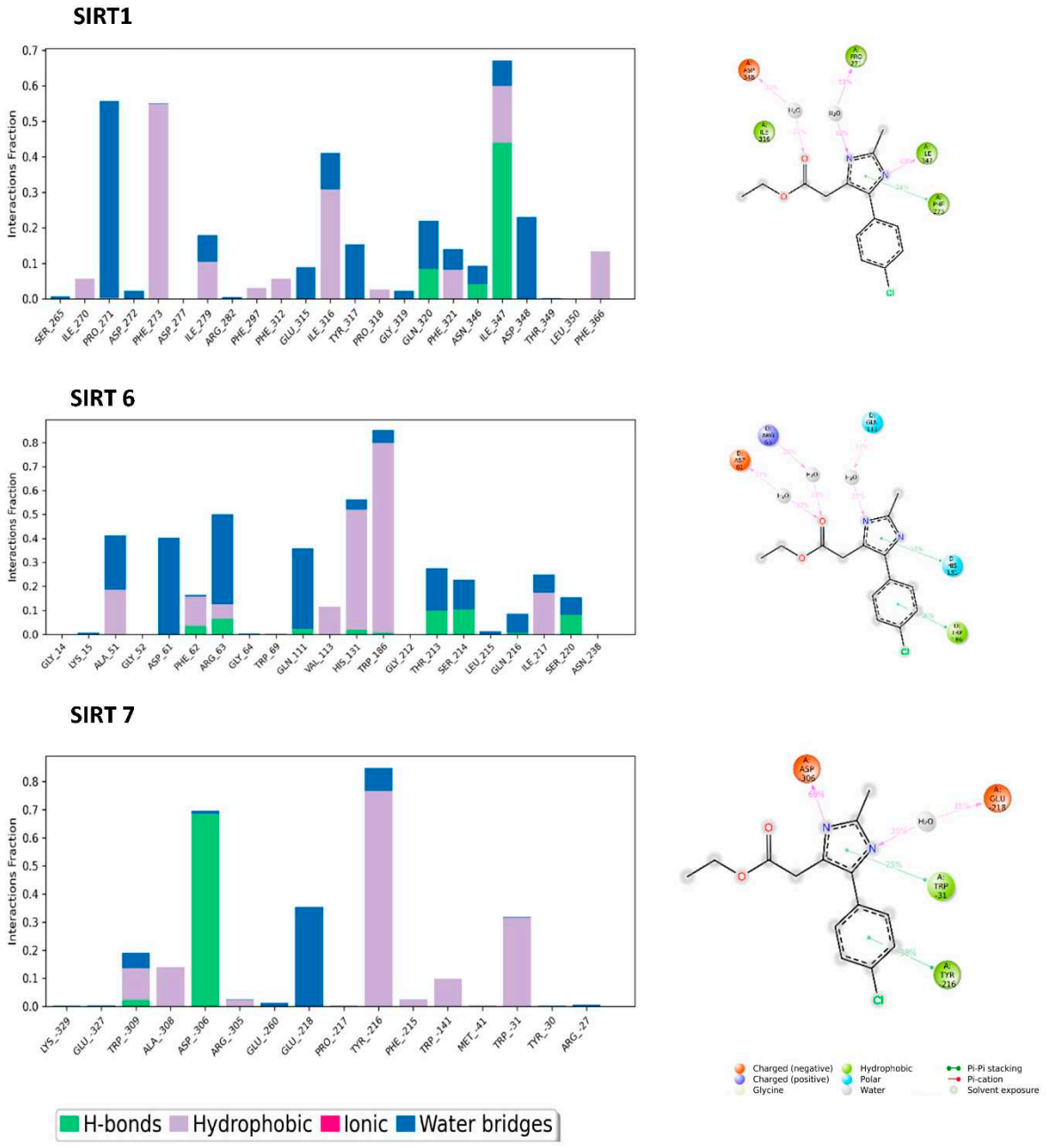

Fig 5. Protein interactions with the ligand can be monitored throughout the simulation. These interactions can be categorized by type and summarized, as shown in the plot which depicts Hydrogen Bonds, Hydrophobic, Ionic and Water Bridges.

A schematic of detailed ligand atom interactions with the protein residues. Interactions that occur more than 20.0% of the simulation time in the selected trajectory (0.00 through 100.00 ns), are shown.

Figure 5. Nuclear sirtuin-ligand interaction.

Preprints (www.preprints.org) | NOT PEER-REVIEWED | Posted: 18 August 2023 doi:10.20944/preprints202308.1350.v1

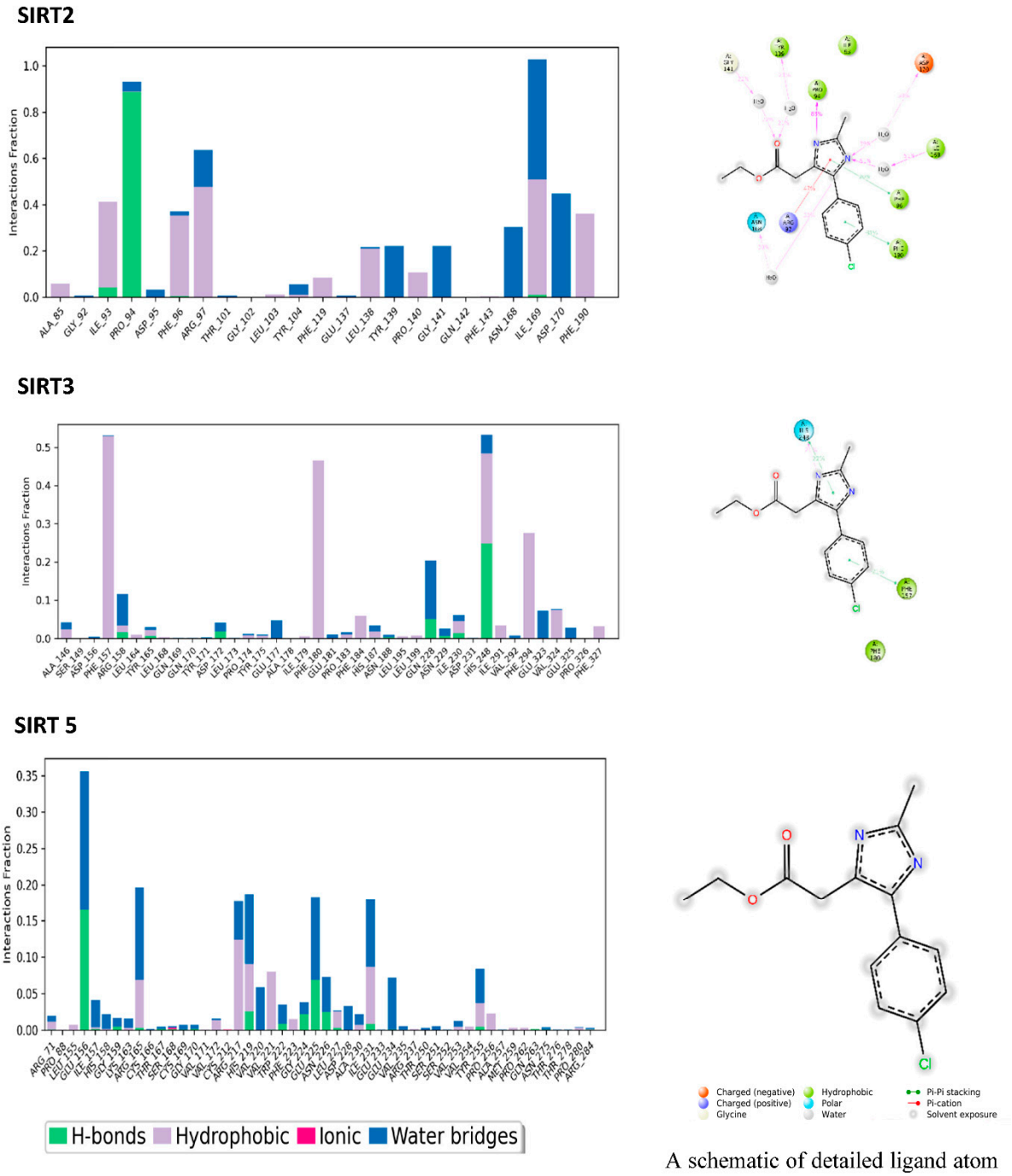

Protein interactions with the ligand can be monitored throughout the simulation. These interactions can be categorized by type and summarized, as shown in the plot which depicts Hydrogen Bonds, Hydrophobic, Ionic and Water Bridges.

A schematic of detailed ligand atom interactions with the protein residues. Interactions that occur more than 20.0% of the simulation time in the selected trajectory (0.00 through 100.00ns), are shown.

Figure 6. Cytoplasmic and Mitochondrial Sirtuin-Ligand Interaction.

3.4. DFT calculation

DFT analysis was carried out to understand the We also calculated the Highest occupied molecular orbital of the ligand which was about -0.27412 and the Least unoccupied molecular orbital was -0.02618 **(Figure 7)**.

Preprints (www.preprints.org) | NOT PEER-REVIEWED | Posted: 18 August 2023 doi:10.20944/preprints202308.1350.v1

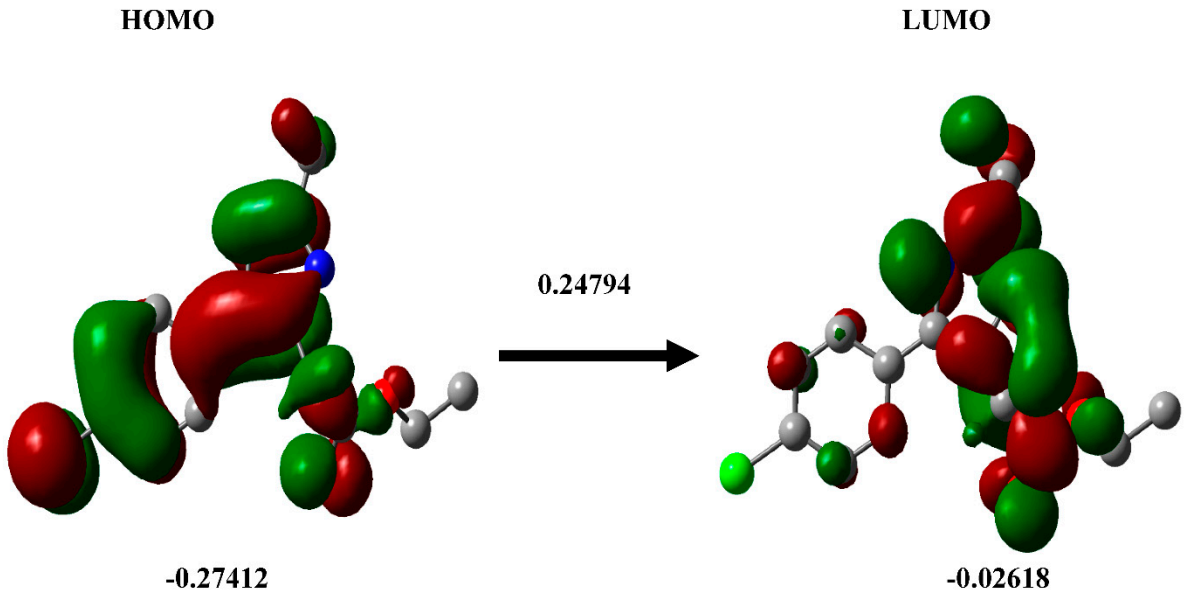

Figure 7. The DFT calculation for the ligand Ethyl 2-[5-(4-chlorophenyl)-2-methyl-1-H-Imidazole-4-yl) acetate calculated is shown. HOMO (Left), LUMO (Right).

3.5. ADME Analysis

ADME properties were analyzed for all the ligands that underwent the study. The results of the ADME analysis show effective absorption, solubility, and the ability of the compound to dwell in the gut-blood barrier and blood-brain barrier **(Table 4)**.

Table 4. ADMET analysis of the Imidazole derivatives in comparison with Imidazole parent Structure: Emphasizing the efficiency of Imidazole derivatives.

Ligand Name	Molecular weight	SASA	FOSA	FISA	Donor HB	Acceptor HB	VOLUME	QPlogPw	QPlogP/w	QPlogBB	QPlogS	QPPCaCO	Human Oral Absorption	%Human Oral Absorption
Acceptable Range	(<500 Da)	(300.0 – 1000.0)	(0.0 – 750.0)	(7.0 – 330.0)	(<5), g)	(<10), h)	(500.0 – 2000.0)	(4.0 – 45.0)	(–2.0-6.5)	(–3.0 – 1.2)	(–6.5-0.5)	(<25 poor, >500 great)	--	(<25% is poor and >80% is high)
Ethyl 2-(2,5-diphenyl-1H-imidazole-4-yl) acetate	306.363	585.302	143.504	73.186	1	3.5	1029.252	8.373	4.212	-5.184	-0.284	2102.639	3	100
Ethyl 2-[2-phenyl-5-(3,4,5-trimethoxyphenyl)-1H-imidazol-4-yl] acetate	396.442	683.134	374.559	72.031	0	4.75	1255.511	6.817	4.951	-5.699	-0.506	2055.082	3	100
Ethyl 2-[5-(4-chlorophenyl)-2-phenyl-1H-imidazol-4-yl] acetate	340.808	646.409	176.469	57.976	1	3.5	1111.022	8.259	5.05	-6.598	-0.041	2793.266	1	100
Ethyl 2-[5-(4-bromophenyl)-2-phenyl-1H-imidazol-4-yl] acetate	385.259	654.421	177.218	57.77	1	3.5	1121.383	8.291	5.14	-6.768	-0.033	2805.877	1	100
Ethyl 2-{2-phenyl-5-[4-(trifluoromethyl) phenyl]-1H-imidazol-4-yl} acetate	374.362	666.352	171.63	59.5	1	3.5	1160.555	8.18	5.504	-7.159	0.054	2701.827	1	100
Ethyl 2-[5-(4-chlorophenyl)-2-methyl-1-H-Imidazole-4-yl) acetate	278.738	558.092	272.468	72.352	1	3.5	933.926	6.793	3.6	-5.01	-0.145	2040.747	3	100
Imidazole	68.078	228.199	0	65.325	1	2	309.474	5.255	-0.08	-0.485	0.1	2379.132	3	86.91

doi:10.20944/preprints202308.1350.v1

Preprints (www.preprints.org) | NOT PEER-REVIEWED | Posted: 18 August 2023 doi:10.20944/preprints202308.1350.v1

3.6. PROTEIN-LIGAND interaction-3D view

3.7. DFT calculation

3.8. Cytotoxicity Effect of Ethyl [5-(4- Chlorophenyl)-2-methyl-1H-imidazol-4-yl}-acetate

The cytotoxicity of Imidazole and its derivative Ethyl [5-(4- Chlorophenyl)-2-methyl-1H-imidazol-4-yl}-acetate is determined in NSCLC cell lines A549 and NIC-H460 using MTT assay. The cells were treated with imidazole and imidazole derivatives with different concentrations for 24 h. The cell viability is decreased gradually with an increase in concentration. The half maximal inhibitory concentration (IC50) of Imidazole and its derivative is found to be 600 µM and 250 µM in the A549 cell line (Figure 8a,b) and 700 µM and 300 µM in the NIC-H460 cell line (Figure 8c,d). Imidazole derivative at lower concentration reduced the cell viability in comparison to parent compound imidazole in NSCLC cell lines.

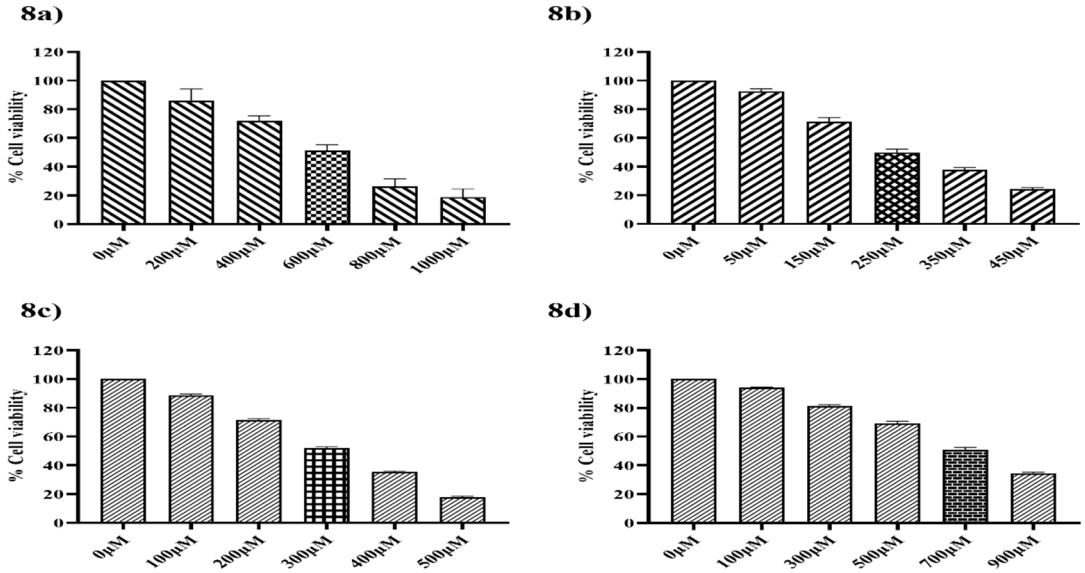

Figure 8. The Cell viability activity of imidazole and imidazole derivative Ethyl [5-(4-Chlorophenyl)-2-methyl-1H-imidazol-4-yl}-acetate with different concertation for a treatment period of 24 h in NSCLC cell lines A549 and NIC-H460 cell lines. The 8a) and 8b) show the cell viability activity of imidazole and imidazole derivatives in the A549 cell line. whereas 8c) and 8d) show the Cell viability activity of imidazole and imidazole derivatives in the NIC-H460 cell line.

3.9. In-Vitro analysis of Imidazole derivative Ethyl [5-(4-Chlorophenyl)-2-methyl-1H-imidazol-4-yl]-acetate effect on Class III Histone deacetylase family (SIRT)

Sirtuins are class III Histone deacetylases with seven isoforms (SIRT1-7). The role of Sirtuins is varied differently depending on the type of cancer. In this study, we explored the effect of imidazole derivative Ethyl [5-(4-Chlorophenyl)-2-methyl-1H-imidazol-4-yl]-acetate in NSCLC cell line A549 and NIC-H460 cell lines. The gene and protein expression studies are carried out to understand the effect of the imidazole derivative. The results from gene expression studies confirm the downregulation of Sirtuins on treatment with Ethyl [5-(4-Chlorophenyl)-2-methyl-1H-imidazol-4-yl]-acetate. Among all the Sirtuins SIRT1, SIRT2 and SIRT6 showed a prominent decrease in expression, followed by other Sirtuins in the order of SIRT3, SIRT5, and SIRT4. SIRT7 was decreased non-significantly. Further western blotting analysis was to carried out to confirm the effect of Ethyl [5-(4-Chlorophenyl)-2-methyl-1H-imidazol-4-yl]-acetate, at the protein level. The expression of all the members of the Sirtuins was decreased on treatment with Ethyl [5-(4-Chlorophenyl)-2-methyl-1H-imidazol-4-yl]-acetate. Among the different isoforms of Sirtuins, SIRT1, and SIRT6 were greatly

Preprints (www.preprints.org) | NOT PEER-REVIEWED | Posted: 18 August 2023 doi:10.20944/preprints202308.1350.v1

affected, followed by SIRT2, SIRT5, SIRT3, and SIRT7. Figure (10) shows the western blot of all the isoforms of Sirtuins. The decreased expression of SIRT1 is different in A549 and H460 cell lines, whereas SIRT6 was decreased to the same extent in A549 and NIC-H460 cell lines.

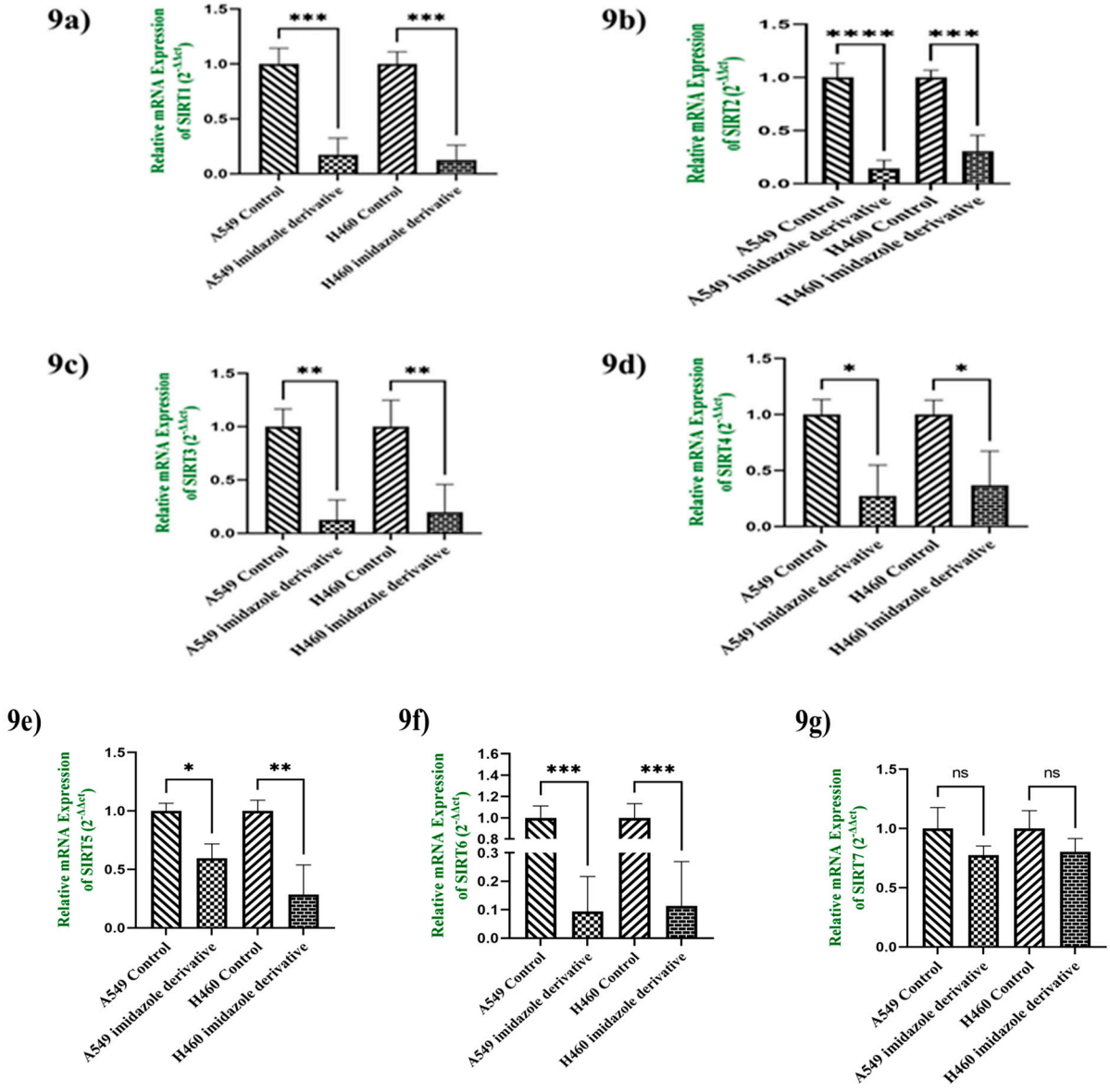

Figure 9. Gene expression of Class III Histone deacetylase family (SIRT1-7) is performed in quantitative Realtime PCR. The graphical representation shows the expression of different sirtuins a) SIRT1, b) SIRT2, c) SIRT3, d) SIRT4, e) SIRT5, f) SIRT6, and g) SIRT7 in NSCLC cell lines A549 and NIC-H460. (Data represent mean values ± SD. *$p < 0.05$, **$p < 0.01$, ***$p < 0.001$ and ****$p < 0.0001$).

Preprints (www.preprints.org) | NOT PEER-REVIEWED | Posted: 18 August 2023 doi:10.20944/preprints202308.1350.v1

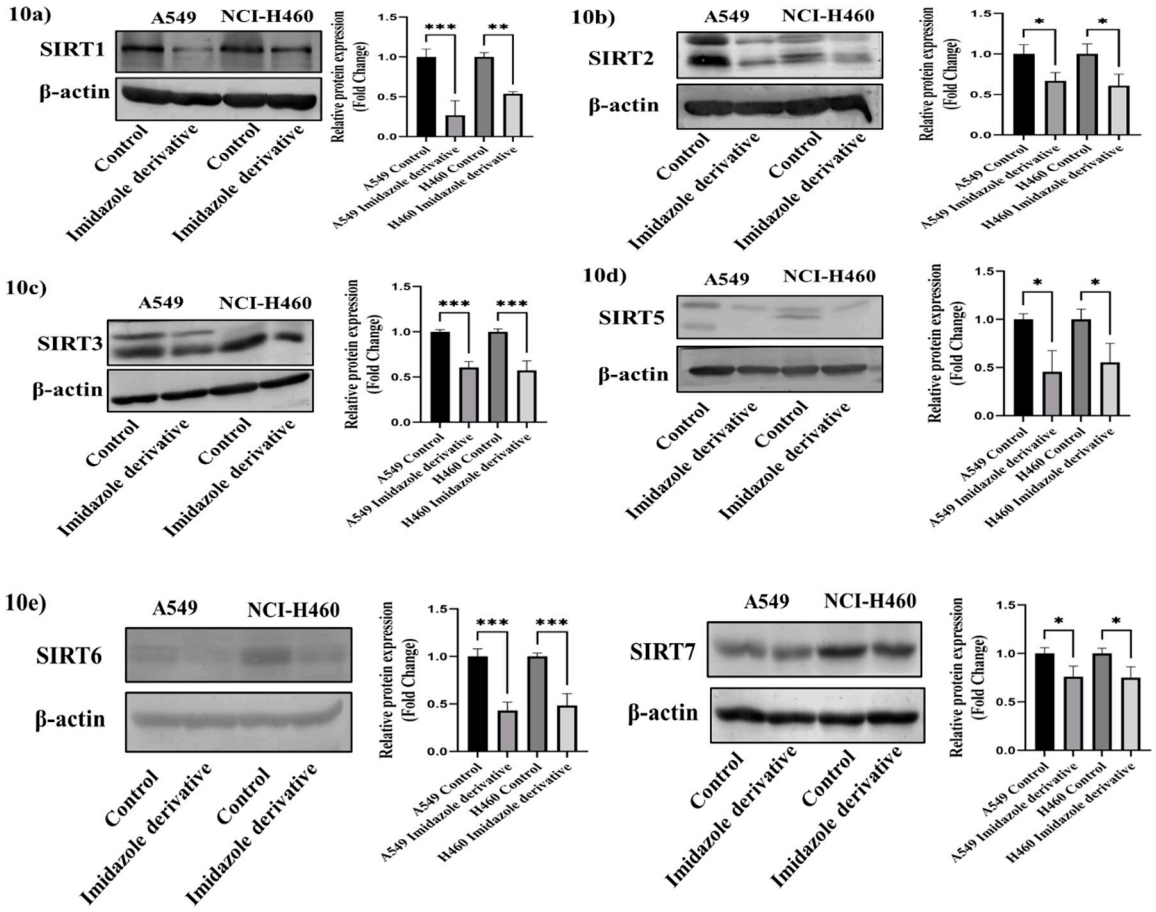

Figure 10. Western blotting is performed to understand the effect of Ethyl [5-(4-Chlorophenyl)-2-methyl-1H-imidazol-4-yl}-acetate on protein expression of Sirtuins. The results show the decrease in expression of a) SIRT1, b) SIRT2, c) SIRT3, d) SIRT5, e) SIRT6, and f) SIRT7 in Ethyl [5-(4-Chlorophenyl)-2-methyl-1H-imidazol-4-yl}-acetate treated NSCLC cell lines A549 and NIC-H460 in comparison with control cells (untreated). β-actin is used as an endogenous control for normalization. Data represent mean values ± SD. *$p < 0.05$, **$p < 0.01$ and ***$p < 0.001$.

4. Discussion

The imidazole derivatives, designed and synthesized in-house were subjected to GLIDE docking analysis from which we can conclude that in spite of cellular localization of the Sirtuins, all the compound structure interacted with the protein, especially the compound Ethyl 2-[5-(4-chlorophenyl)-2-methyl-1-H-Imidazole-4-yl) assures the binding with all the six sirtuin protein (Table 1). The glide gscore depicts that, this compound is more affinitive towards the nuclear sirtuins -Sirt1, Sirt6, and Sirt7 (**-7.807, -6.544, -5.616**) and Cytosolic Sirtuin Sirt2 (**-8.835**). The binding pockets of the protein comprise a set of amino acids (Isoleucine, Alanine, Phenylalanine, Tyrosine, Tryptophan, Glutamate, Histidine, Arginine, and Aspartate) which form effective hydrogen bonds, pi-pi interaction with the ligand (**Figures 1 and 2)**. Sirt1, Sirt6, Sirt7, and Sirt2 depicted more hydrogen bond interactions, whereas the Mitochondrial Sirtuin as Sirt3 and Sirt5 possess the least interactive bonds. Through the RMSD data, we measured the average distance between the atoms of a simulated protein-ligand structure and a reference protein structure and quantified the structural changes of the molecule during the simulation. Using Root Mean Square Deviation (RMSD) data, we determined the average distance between atoms in a simulated protein-ligand structure and a reference protein structure [20]. This quantifies the structural changes in the molecule during the simulation, commonly used to assess simulation stability and convergence **(Figure 3)**. Root Mean Square Fluctuation (RMSF) values were also calculated to understand the average deviation of atom

 doi:10.20944/preprints202308.1350.v1

positions from their mean during the simulation, providing insights into the flexibility and dynamic behavior of various biomolecule regions **(Figure 4) [21]**. In the context of Molecular Dynamics (MD) simulations, studying ligand interactions involves examining how a small molecule (ligand) interacts with a larger biomolecule (e.g., protein or nucleic acid). These interactions encompass hydrogen bonding, van der Waals forces, electrostatic interactions, and more. Understanding these interactions can offer insights into binding strength, binding sites, and potential mechanisms of action **(Figures 5 and 6)**. The interaction of our protein with the ligand underscores its versatile binding potential with all sirtuins. Sirtuins are interconnected HDAC enzymes and they act in turns to achieve pathway activation and inhibition. For instance, multiple studies have reported that Sirtuin 1 possesses power over other nuclear sirtuins. In the case of Double-stranded Break repair mechanisms, SIRT1 facilitates the mobilization of Sirt6 to DSBs by deacetylation [22]. One report suggests that SIRT1 and SIRT6 can bind to the N terminal and C terminal of the Suv39h protein and regulate the repressor pathway of IkBα expression [23]. In contrast, there are research reports stating the importance of Sirt6 in regulating the random acetylation of Sirtuin 1 with respect to Lung cancer. Sirtuin 1 can acetylate/deacetylate and regulate multiple pathways in lung cancer like acetylation of AMP [24], AKT [25], PPAR γ [26], and more. Our gene expression and Protein expression data suggest that the compound Ethyl 2-[5-(4-chlorophenyl)-2-methyl-1-H-Imidazole-4-yl) acetate being well co-operated into the nuclear sirtuins, this can favor the inhibition of nuclear sirtuins and activation of tumor suppression pathways. Inhibition of nuclear sirtuins can clearly affect the other sirtuin actions. The HOMO energy level represents the energy of the highest electron orbital that contains electrons in the molecule. It signifies the energy required to remove an electron from the highest occupied orbital. A lower (more negative) HOMO energy indicates that electrons are relatively tightly bound, which implies that the molecule is less likely to readily donate electrons. In terms of chemical reactivity, the HOMO energy level is associated with the molecule's ability to act as an electron donor in chemical reactions [27]. In Our, a HOMO energy of -0.27412 suggests that the highest occupied electron orbital is relatively lower in energy, indicating that electrons are somewhat tightly bound and less likely to be readily donated. The LUMO energy level represents the energy of the lowest unoccupied electron orbital in the molecule. It indicates the energy required to promote an electron from the highest occupied orbital to this unoccupied orbital [28]. A higher (less negative) LUMO energy suggests that electrons are relatively loosely bound, implying that the molecule can more easily accept electrons. The LUMO energy level is associated with the molecule's ability to act as an electron acceptor in chemical reactions. With a LUMO energy of -0.02618, Our molecule's lowest unoccupied electron orbital is relatively higher in energy, indicating that electrons are somewhat loosely bound and the molecule has a propensity to accept electrons (Figure 7). In the domain of surface area analysis, several crucial components were assessed, including the Total Solvent Accessible Surface Area (SASA), which accounts for the overall surface area available to solvents. Additionally, the hydrophobic component of SASA, known as FOSA, and its counterpart, the hydrophilic component called FISA, were examined [29]. The evaluation of these components yielded values that largely fell within an acceptable range, as stipulated in the Qikprop manual provided by Schrödinger. In particular, the software's guidelines were referenced to ensure that the values obtained for SASA, FOSA, FISA, PISA, and volume align with the established standards. Furthermore, the predictive permeability of the compounds was a focal point of investigation. This was achieved through the utilization of two key metrics: QPPCaco, a model designed for assessing gut-blood barrier permeability [30], and QPlogBB, which pertains to the brain-blood partition coefficient [31]. It was noted that QPPCaco values exceeding 500 are indicative of favorable permeability characteristics. From observation, all of the selected Imidazole derivatives demonstrated values that surpassed the defined range. This conclusion was drawn from a comprehensive analysis and is succinctly presented in **Table 2**, thereby highlighting the compounds' promising potential in terms of permeability. From the ADME analysis and the docking Score, the Imidazole derivative namely Ethyl [5-(4-Chlorophenyl)-2-methyl-1H-imidazol-4-yl]-acetate has greater interaction with the Sirtuins family compared to the imidazole (Table1). Based on the Insilco result, we carried out in-vitro studies with Ethyl [5-(4-Chlorophenyl)-2-methyl-1H-imidazol-4-yl]-acetate to explore its inhibitory effect on

Sirtuin family members (SIRT1-7). Initially, we carried MTT assay to fix the IC_{50} concentration of the Ethyl [5-(4-Chlorophenyl)-2-methyl-1H-imidazol-4-yl]-acetate. The MTT results of Imidazole alone and Imidazole derivative show that Imidazole derivative has much effect at lower concentration in 24 h of treatment in A549 (250μM) and NIC-H460 (300μM) in comparison to the parent imidazole compound in A549 (600μM) and NIC-H460 (700 μM) cell lines. Further, the gene and protein expression studies were carried out with IC_{50} concentration of imidazole derivative Ethyl [5-(4-Chlorophenyl)-2-methyl-1H-imidazol-4-yl]-acetate. The gene expression results from qRT-PCR confirm the decrease in the expression of sirtuins in NSCLC cell line A549 and NIC-H460. Among the Sirtuins SIRT1, SIRT2 and SIRT6 were greatly reduced on Ethyl [5-(4-Chlorophenyl)-2-methyl-1H-imidazol-4-yl]-acetate, followed by SIRT3, SIRT5 and SIRT6. SIRT7 expression decreased non-significantly. The results from western blot analysis also confirm the decreased expression of sirtuins which correlated with gene expression of sirtuins. Among the sirtuins, the protein expression of SIRT1 and SIRT6 has greatly reduced which was correlated with gene expression of SIRT1 and SIRT6.

5. Conclusion:

Cancer being an indestructible target for biologists, every day new drugs are out in the market. But the potentially regulating compounds are scarcely found. Our in-house compounds have established potential interaction with epigenetic-modulating sirtuin enzymes that can inhibit cancer progression. Our In-silico data shows that the imidazole derivative Ethyl [5-(4-Chlorophenyl)-2-methyl-1H-imidazol-4-yl]-acetate perfects the Lipinski rule of five and possess high docking score which confirms the interaction with all the Sirtuin isoforms. The Dynamics data further confirms the stability of the bound ligand with the protein. In correspondence to the in-silico study, the results from the invitro study confirm the inhibitory effect of imidazole derivative, Ethyl [5-(4-Chlorophenyl)-2-methyl-1H-imidazol-4-yl]-acetate. Taken together, our results demonstrate the concurrent data in both in-silico and invitro analysis where the imidazole derivative is highly effective upon nuclear sirtuins SIRT1, SIRT6, and cytosolic sirtuin SIRT2, followed by other members of the sirtuins SIRT3, SIRT5, and SIRT7. Thus, from the above in-silico and in-vitro studies, we claim our in-house imidazole derivative Ethyl [5-(4-Chlorophenyl)-2-methyl-1H-imidazol-4-yl]-acetate as a potential inhibitor of Class III HDACs, in particular to SIRT1, SIRT6, and SIRT2.

Author Contributions: Conceptualization: R.V., D.U.M.R., and T.R. Study Design and execution: D.U.M.R., S.P.S. Data analysis and summary: S.A.G., N.A.A., S.B.D., A.A.A., M.S. Writing original draft: D.U.M.R., R.V. Writing review& editing: D.U.M.R., R.V.

Funding: Self.

Ethics approval and consent to participate: Not applicable.

Consent for publication: All authors consented to publish this study.

Availability of data and materials: Sets of data or summaries generated during the present study are available from the corresponding author upon reasonable request.

Acknowledgments: The authors acknowledge the RUSA-2.0 (Biological Sciences, BDU), DST-PURSE Phase II, and, DST-FIST, Government of India for their support in providing funds for the improvement of instrumentation facilities in our department. The authors would also like to acknowledge a research grant from the Indian Council of Medical Research (ICMR), New Delhi, India. (Ref. No: 52/13/2020-BIO-BMS and Ref. No: VIR/ COVID-19/6/2021/ECD-I). We wish to acknowledge Dr. K. Srinivasan, Professor, School of Chemistry, Bharathidasan University for providing the Imidazole derivative which was used in the present study.

Competing interests: The authors declare no competing interests.

Compliance with Ethical Standards

Disclosure of potential conflicts of interest: The authors declare that there is no conflict of interest.

Research involving human participants and/or animals: Not applicable.

Informed consent: Not applicable.

Abbreviations

HDAC, Histone Deacetylase; NSCLC, Non-Small Cell Lung Cancer; SIRT (1-7), Sirtuins (1-7); NAD, Nicotinamide Adenine Dinucleotide; PDB, Protein Data Bank; RCSB, Research Collaboratory for Structural Bioinformatics; OPLS, Optimized Potentials for Liquid Simulations; GLIDE, Grid-Based Ligand Docking with Energetics; MDS, Molecular Dynamics Simulation; DESMOND: Desmond, Molecular Dynamics System; TIP3P, Transferable Intermolecular Potential with 3 Points; RMSD, Root Mean Square Deviation; RMSF, Root Mean Square Fluctuation; DFT, Density Functional Theory; ADME, Absorption, Distribution, Metabolism, Excretion; Ligprep, Ligand Preparation; B3LYP-D3, Becke 3-parameter hybrid functional combined with Lee-Yang-Parr correlation functional and D3 dispersion correction; HOMO, Highest Occupied Molecular Orbital; LUMO, Lowest Unoccupied Molecular Orbital; SASA, Solvent Accessible Surface Area; FISA, Flexible Inhibitor Surface Anchoring; FOSA, Force-Field Overlapping Scoring Algorithm; QPlog BB, Quantum Polarized Ligand-Based Binding Energy; QPlogS, Quantum Polarized Surface Area Solvation Energy; QplogPw, Quantum Polarized Water-Octanol Partitioning Energy; QPPCaCO, Quantum Polarized Partial Charge of Carbon in Carbonyl; HB, Hydrogen Bond.

References

1. Ali I, Lone MN, Aboul-Enein HY. Imidazoles as potential anticancer agents. MedChemComm. 2017;8(9):1742-73.
2. Sharma P, LaRosa C, Antwi J, Govindarajan R, Werbovetz KA. Imidazoles as potential anticancer agents: An update on recent studies. Molecules. 2021 Jul 11;26(14):4213.
3. Bryaskova R, Georgiev N, Philipova N, Bakov V, Anichina K, Argirova M, Apostolova S, Georgieva I, Tzoneva R. Novel Fluorescent Benzimidazole-Hydrazone-Loaded Micellar Carriers for Controlled Release: Impact on Cell Toxicity, Nuclear and Microtubule Alterations in Breast Cancer Cells. Pharmaceutics. 2023 Jun 16;15(6):1753.
4. Rajabi M, Mousa S. The Role of Angiogenesis in Cancer Treatment. Biomedicines [Internet]. 2017; 5:34. Available from: http://dx.doi.org/10.3390/biomedicines5020034
5. Azad A, Kong A. The Therapeutic Potential of Imidazole or Quinone-Based Compounds as Radiosensitisers in Combination with Radiotherapy for the Treatment of Head and Neck Squamous Cell Carcinoma. Cancers. 2022 Sep 27;14(19):4694.
6. Tolomeu HV, Fraga CA. Imidazole: Synthesis, Functionalization and Physicochemical Properties of a Privileged Structure in Medicinal Chemistry. Molecules. 2023 Jan 13;28(2):838.
7. Sharma A, Kumar V, Kharb R, Kumar S, Chander Sharma P, Pal Pathak D. Imidazole derivatives as potential therapeutic agents. Current pharmaceutical design. 2016 Jun 1;22(21):3265-301.
8. Kandasamy S, Subramani P, Srinivasan K, marshal Jayaraj J, Prasanth G, Muthusamy K, Rajakannan V, Vilwanathan R. Design and synthesis of imidazole-based zinc binding groups as novel small molecule inhibitors targeting Histone deacetylase enzymes in lung cancer. Journal of Molecular Structure. 2020 Aug 15;1214:128177.
9. Dai H, Sinclair DA, Ellis JL, Steegborn C. Sirtuin activators and inhibitors: Promises, achievements, and challenges. Pharmacology & therapeutics. 2018 Aug 1;188:140-54.
10. Zhu S, Dong Z, Ke X, Hou J, Zhao E, Zhang K, Wang F, Yang L, Xiang Z, Cui H. The roles of sirtuins family in cell metabolism during tumor development. InSeminars in cancer biology 2019 Aug 1 (Vol. 57, pp. 59-71). Academic Press.
11. Chi B. Vu, Jean E. Bemis, Jeremy S. Disch, Pui Yee Ng, Joseph J. Nunes, Jill C. Milne, David P. Carney, Amy V. Lynch, Jesse J. Smith, Siva Lavu, Philip D. Lambert, David J. Gagne, Michael R. Jirousek, Simon Schenk, Jerrold M. Olefsky, and Robert B. Perni
    a. Journal of Medicinal Chemistry 2009 52 (5), 1275-1283
    b. DOI: 10.1021/jm8012954.
12. Morris BJ, Willcox BJ, Donlon TA. Genetic and epigenetic regulation of human aging and longevity. Biochimica et Biophysica Acta (BBA)-Molecular Basis of Disease. 2019 Jul 1;1865(7):1718-44.
13. Chalkiadaki A, Guarente L. The multifaceted functions of sirtuins in cancer. Nature Reviews Cancer. 2015 Oct;15(10):608-24.
14. Bosch-Presegué L, Vaquero A. The dual role of sirtuins in cancer. Genes Cancer. 2011 Jun;2(6):648-62. doi: 10.1177/1947601911417862. PMID: 21941620; PMCID: PMC3174263.
15. Alcaín FJ, Villalba JM. Sirtuin inhibitors. Expert opinion on therapeutic patents. 2009 Mar 1;19(3):283-94.
16. Jiang Y, Liu J, Chen D, Yan L, Zheng W. Sirtuin inhibition: strategies, inhibitors, and therapeutic potential. Trends in pharmacological sciences. 2017 May 1;38(5):459-72.

17. Hu J, Jing H, Lin H. Sirtuin inhibitors as anticancer agents. Future Med Chem. 2014 May;6(8):945-66. doi: 10.4155/fmc.14.44. PMID: 24962284; PMCID: PMC4384657.
18. Wu, QJ., Zhang, TN., Chen, HH. et al. The sirtuin family in health and disease. Sig Transduct Target Ther 7, 402 (2022). https://doi.org/10.1038/s41392-022-01257-8
19. Krishnamoorthy V, Vilwanathan R. Silencing Sirtuin 6 induces cell cycle arrest and apoptosis in non-small cell lung cancer cell lines. Genomics. 2020 Sep 1;112(5):3703-12.
20. Kirchmair J, Markt P, Distinto S, Wolber G, Langer T. Evaluation of the performance of 3D virtual screening protocols: RMSD comparisons, enrichment assessments, and decoy selection—what can we learn from earlier mistakes?. Journal of computer-aided molecular design. 2008 Mar;22:213-28.
21. Margreitter C, Oostenbrink C. MDplot: visualise molecular dynamics. The R journal. 2017 May 10;9(1):164.
22. Meng F, Qian M, Peng B, Peng L, Wang X, Zheng K, Liu Z, Tang X, Zhang S, Sun S, Cao X. Synergy between SIRT1 and SIRT6 helps recognize DNA breaks and potentiates the DNA damage response and repair in humans and mice. elife. 2020 Jun 15;9:e55828.
23. Santos-Barriopedro I, Bosch-Presegué L, Marazuela-Duque A, de la Torre C, Colomer C, Vazquez BN, Fuhrmann T, Martínez-Pastor B, Lu W, Braun T, Bober E. SIRT6-dependent cysteine monoubiquitination in the PRE-SET domain of Suv39h1 regulates the NF-κB pathway. Nature communications. 2018 Jan 9;9(1):101.
24. Park SJ, Ahmad F, Philp A, Baar K, Williams T, Luo H, Ke H, Rehmann H, Taussig R, Brown AL, Kim MK. Resveratrol ameliorates aging-related metabolic phenotypes by inhibiting cAMP phosphodiesterases. Cell. 2012 Feb 3;148(3):421-33.
25. Pillai VB, Sundaresan NR, Gupta MP. Regulation of Akt signaling by sirtuins: its implication in cardiac hypertrophy and aging. Circ Res. 2014 Jan 17;114(2):368-78. doi: 10.1161/CIRCRESAHA.113.300536. PMID: 24436432; PMCID: PMC4228987.
26. Qiang L, Wang L, Kon N, Zhao W, Lee S, Zhang Y, Rosenbaum M, Zhao Y, Gu W, Farmer SR, Accili D. Brown remodeling of white adipose tissue by SirT1-dependent deacetylation of Pparγ. Cell. 2012 Aug 3;150(3):620-32.
27. Prabhaharan M, Prabakaran AR, Gunasekaran S, Srinivasan S. DFT studies on vibrational spectra, HOMO–LUMO, NBO and thermodynamic function analysis of cyanuric fluoride. Spectrochimica Acta Part A: Molecular and Biomolecular Spectroscopy. 2015 Feb 5;136:494-503.
28. Mathammal R, Jayamani N, Geetha N. Molecular structure, NMR, HOMO, LUMO, and vibrational analysis of O-anisic acid and anisic acid based on DFT calculations. Journal of Spectroscopy. 2013 Oct;2013.
29. Fatima S, Gupta P, Sharma S, Sharma A, Agarwal SM. ADMET profiling of geographically diverse phytochemical using chemoinformatic tools. Future medicinal chemistry. 2020 Jan;12(1):69-87.
30. Telvekar VN, Bairwa VK, Satardekar K, Bellubi A. Novel 2-(2-(4-aryloxybenzylidene) hydrazinyl) benzothiazole derivatives as anti-tubercular agents. Bioorganic & medicinal chemistry letters. 2012 Jan 1;22(1):649-52.
31. Jhala DD, Chettiar SS, Singh JK. Optimization and Validation of an In Vitro Blood Brain Barrier Permeability Assay Using Artificial Lipid Membrane.